Fusion Engineering and Design 234 (2027) 116133

Contents lists available at ScienceDirect

Fusion Engineering and Design

journal homepage: www.elsevier.com/locate/fusengdes

Design considerations on coaxial gyrotron cavities for MW-class continuous-wave dual-harmonic operation

Elena Katsara [a,*], Konstantinos A. Avramidis [a], Ioannis Chelis [a], Chuanren Wu [b], Jianbo Jin [b], Lukas Feuerstein [b], Charilaos Argyropoulos [a], Manfred Thumm [b], Stefan Illy [b]

[a] National and Kapodistrian University of Athens, Department of Physics, Athens, Greece
[b] Karlsruhe Institute of Technology, Institute for Pulsed Power and Microwave Technology, Germany

ARTICLE INFO

Keywords:
Coaxial-cavity gyrotron
Harmonic gyrotron
Dual-harmonic operation
Electron cyclotron resonance heating

ABSTRACT

In the need for development of megawatt-class gyrotrons capable of ultra-fast switching between two widely separated operating frequencies, which will allow the same device to deliver power both for Electron Cyclotron Resonance Heating (ECRH) and rapid Radiative Instability Suppression in fusion reactors, essential considerations are presented. They refer to the operating-mode selection and to the design of a coaxial-cavity for stable Continuous-Wave (CW) operation at both the fundamental cyclotron frequency and the second cyclotron harmonic. Tools for the selection of the appropriate operating mode pair are developed, taking into account window reflections, compatibility with the quasi-optical output coupler, Ohmic wall loading, and the need for rapid switching between the two cyclotron harmonics. The required ultra-fast switching (in the range of milliseconds) between the two widely separated operating frequencies is possible by changing only the voltage values in a triode-type electron gun configuration. On this basis, and using the developed tools, a coaxial cavity that supports dual-harmonic CW operation and generates an RF power of around 1.3 MW both at 170 GHz and at 85 GHz is designed and validated by multi-mode simulations. An ultra-fast switching scenario is also demonstrated. The presented results point towards the feasibility of dual-harmonic MW-class gyrotrons, which are expected to reduce the overall cost and space requirements of the ECRH installations.

1. Introduction

In magnetically-confined fusion plasma experiments, gyrotrons are the only known high power sources today that are capable of continuously delivering the required megawatt-level microwave power in Electron Cyclotron (EC) Heating and Current Drive (HCD) system for plasma start-up, heating the fusion plasma to burn as well as controlling and stabilizing the plasma during a discharge [1,2]. In addition, gyrotrons also generate the incident mm-waves required for diagnostic techniques such as Collective Thomson Scattering, which provide essential insights into plasma parameters and behavior [3,4].

The RF power emitted by gyrotrons is absorbed within the plasma at EC resonances. The cyclotron frequency is determined by the magnetic field and since the magnetic field varies across the cross section of the toroidal plasma in a known way - essentially inversely proportional to the major radius of the torus - the location of the resonance with a given frequency can be well estimated. Consequently, the deposition of EC-wave power at different plasma locations could be achieved by distinct wave frequencies. In the context of future reactors, each frequency will require the installation of several tens of gyrotrons to achieve the necessary total power and system reliability. Considering that a single gyrotron, including its superconducting magnet and high voltage power supply, costs several million euro – excluding the associated transmission and launching subsystems – the total number of gyrotrons becomes a decisive factor in the overall HCD system cost and architectural optimization.

According to recent HCD functional requirements for a future EU fusion reactor [2,5], an EC power of approximately 70 MW is proposed to be deployed to mitigate Radiative Instabilities (RIs). These instabilities are primarily induced by small tungsten particles eroded from plasma-facing components. When they fall into the plasma a burst of impurity radiation is causing a rapid drop in electron temperature at the plasma edge. If this cooling effect is not quickly countered by localized HCD, it can trigger a chain of events that ultimately leads to plasma

* Corresponding author.
E-mail address: ekatsara@phys.uoa.gr (E. Katsara).

https://doi.org/10.1016/j.fusengdes.2026.116133
Received 1 July 2026; Received in revised form 18 September 2026; Accepted 30 October 2026
0920-3796/© 2026 The Author(s). Published by Elsevier B.V. This is an open access article under the CC BY license (http://creativecommons.org/licenses/by/4.0/).
Open access publication of this article was funded by HEAL-Link under an agreement between Elsevier and HEAL-Link

disruption [6]. To prevent RIs, gyrotrons operating at lower frequency, of the order of half the frequency used for plasma heating, are necessary. However, constructing a dedicated system solely for RI control is challenging. Such a configuration would require a substantial amount of standby power, occupy valuable space, and introduce additional complexity to the already intricate HCD infrastructure. Furthermore, gyrotrons kept on standby for extended periods will not avoid emitter degradation due to sustained thermal loading, thus requiring similar maintenance to that of the gyrotrons used more regularly.

A promising solution to these challenges would be the development of gyrotrons capable of fast switching between two widely separated operating frequencies, allowing the same device to deliver power both for typical EC HCD operation (e.g. heating and localized current drive for mitigation of neoclassical tearing modes) and for rapid RI suppression. This could be realized by operating the same gyrotron at different harmonics of the electron cyclotron frequency. Reflecting the interest in this concept, the dedicated EUROfusion Enabling Research Grant ENR-TEC.02.KIT-T002-D001 [7], jointly undertaken by KIT and NKUA, has been launched to explore this possibility. Parts of this research are presented in this paper.

The feasibility of megawatt-class second harmonic gyrotrons using the coaxial cavity concept has already been demonstrated theoretically [8,9], by exploiting the capability of the coaxial insert to harness mode competition, especially from modes interacting at the fundamental cyclotron frequency. Building on this foundation, the investigation presented in this paper seeks to enable intentional, fast and controlled transition between (a) gyrotron operation at the fundamental cyclotron frequency for RI suppression at frequency f_1 and (b) gyrotron operation at the second cyclotron harmonic for typical EC HCD at frequency $f_2 \cong 2f_1$. Achieving such capability requires a resonant cavity that can accommodate two operating modes, one for each harmonic, ensuring that (a) the fundamental mode does not dominate or suppress the second-harmonic mode during typical EC HCD operation, which is possible only in the presence of the coaxial insert, and (b) the second-harmonic mode does not disturb the operation with the fundamental mode during operation for RI suppression. As already discussed, the realization of such dual-harmonic gyrotrons would provide a new degree of flexibility in EC-system design, reducing the number of gyrotrons and transmission lines required and simplifying the overall architecture of the system. To theoretically demonstrate the feasibility of high-power dual-harmonic operation with fast switching, the frequency pair of 170 GHz and 85 GHz has been selected in this work. The motivation for this choice has been the existing and extensive theoretical and experimental experience with MW-class 170 GHz gyrotrons as well as the consideration of 170 GHz as the primary ECRH frequency in ITER and other upcoming fusion reactors.

In this paper, first a theoretical approach is presented in Section 2 that addresses two primary challenges: (1) maintaining similar performance at both harmonics with the same gyrotron quasi – optical system, electron gun and output window, and (2) ensuring stable Continuous-Wave (CW) operation for both the fundamental and the second-harmonic mode in different voltage ranges. The above two requirements are satisfied through the identification of suitable operating mode pairs that satisfy appropriate conditions. The Ohmic losses in the coaxial cavity play a critical role in selecting the appropriate mode pair. Contour plots derived from generalized mathematical expressions indicate that the mode pairs capable of supporting powerful CW mm-wave operation are limited by the technological constraints with respect to the cooling of the outer cavity wall and the coaxial insert. Single-mode simulations of the electron beam wave interaction are also performed in this Section and serve as an additional validation of the use of the generalized contour plots for the correct selection of operating mode pairs. Section 3 proposes a coaxial cavity design capable of supporting fast switching between cyclotron harmonics, while ensuring good interaction efficiency at both harmonics. Multi-mode simulations of the beam-wave interaction demonstrate stable CW operation for both the fundamental and the second harmonic mode. Finally, the conclusions of this work are summarized in Section 4.

2. Candidate mode pairs for dual-harmonic operation

2.1. Basic requirements

In a gyrotron cavity, radiation is generated from the resonant interaction between an annular beam of gyrating electrons and a Transverse Electric (TE) mode of the electromagnetic field, close to cutoff. The interaction is governed by the resonance condition

$$\omega \approx s\omega_c, s = 1, 2, \tag{1}$$

where ω is the wave angular frequency, ω_c is the relativistic electron cyclotron frequency, and s the integer harmonic number that expresses the harmonic of the electron cyclotron motion with which the electromagnetic wave is synchronized. This resonance condition allows the operating frequency to be tuned either by adjusting the magnetic field (which cannot be done fast) or by switching the harmonic number of the interaction. For $s = 1$, the interaction occurs at the fundamental cyclotron frequency (i.e. first-harmonic operation), whereas for $s = 2$, the resonance corresponds to the second harmonic of the cyclotron frequency (i.e. second-harmonic operation).

The concept of a dual-harmonic gyrotron is based on two operating modes. The first mode, $TE^{(1)}_{m_1,p_1}$ interacts with the electron beam at the fundamental cyclotron frequency whereas the second mode, $TE^{(2)}_{m_2,p_2}$, interacts at the second harmonic of the cyclotron frequency. The indices m_i and p_i are the azimuthal and radial index of the $TE^{(s)}_{m_i,p_i}$ mode, respectively. For simplicity, after this point the explicit indices are intentionally avoided, and the operating modes are denoted as $TE^{(1)}$ and $TE^{(2)}$. The interaction with the $TE^{(2)}$, generates radiation for typical EC HCD with a frequency $f^{(2)}$ whereas, for RI control, a lower frequency of

$$f^{(1)} = \frac{f^{(2)}}{2} + \Delta f \tag{2}$$

can be generated by $TE^{(1)}$. Δf should approach zero, to achieve an optimal transmission with minimum reflections from the gyrotron window, for both harmonics/modes. This is so because, to avoid reflections of a wave from the gyrotron window, the window thickness d_{window} should be equal to an integer number of half wavelengths [10]

$$d_{\text{window}} = N\frac{\widetilde{\lambda}}{2},\ N = 1,\ 2,\ 3, \tag{3}$$

where $\widetilde{\lambda} = \lambda/\sqrt{\varepsilon_r}$ is the wavelength of the TE mode in the window material, λ is the free-space wavelength and ε_r the relative permittivity of the dielectric.

Megawatt-class, long-pulse gyrotrons employ synthetic diamond windows fabricated by Chemical Vapor Deposition (CVD) [10–12]. CVD diamond has a relative permittivity of $\varepsilon_r = 5.67$ and a very low loss tangent $\tan\delta \approx 2 \times 10^{-5}$. The basic formalism for disk-type windows for gyrotrons based on the scattering matrix formulation is presented in [10]. The reflection coefficient, assuming the propagation of a quasi-TEM wave of frequency f through a lossless window ($\tan\delta \ll 1$) of thickness d_{window} can be expressed as [10]:

$$R = \frac{2|\rho_n|^2\left(1 - \cos\left(4\pi f\sqrt{\varepsilon_r}\ d_{\text{window}}\ /\ c\right)\right)}{1 - 2|\rho_n|^2\cos\left(4\pi f\sqrt{\varepsilon_r}\ d_{\text{window}}\ /\ c\right) + |\rho_n|^4}, \tag{4}$$

where $\rho_n = (1 - \sqrt{\varepsilon_r})/(1 + \sqrt{\varepsilon_r})$.

For this study, it is assumed that d_{window} is selected to enable perfect transmission ($R^{(2)} = 0$) of the second-harmonic mode, i.e. $d_{\text{window}} = N\widetilde{\lambda}^{(2)}/2$, where N should be equal to an even integer number to allow good transmission also of the first-harmonic mode. Consequently, (4) is

used only for the calculation of the reflection coefficient of the fundamental $TE^{(1)}$ mode. By replacing the frequency f with $f^{(1)}$ from (2) and considering that Δf approaches zero, a second-order Taylor expansion can be used for the cosine

$$\cos\left[2\pi N\left(\frac{\Delta f}{f^{(2)}}\right)\right] \doteq \cos x \approx 1-\frac{x^2}{2}. \quad (5)$$

Also, for a $TE^{(1)}$ mode near cutoff we have $f^{(1)} \cong c\chi^{(1)}/(2\pi R_o)$, where the eigenvalue $\chi^{(1)}$ of the mode is the p-th root of the characteristic equation $J_m'(\chi^{(1)}) = 0$, and R_o is the outer radius of the cavity. From the above, the reflection coefficient for $TE^{(1)}$ can be written as:

$$R^{(1)} = \left(\frac{\pi N(1-\varepsilon_r)}{2\sqrt{\varepsilon_r}\,\chi^{(2)}}\Delta\chi\right)^2, \quad (6)$$

where $\chi^{(2)} = 2\chi^{(1)} + \Delta\chi$ is the eigenvalue of the $TE^{(2)}$ mode and $\Delta\chi$ should be as close as possible to zero. Indeed, the expression (6) indicates that if $\Delta\chi$ and consequently Δf gets large, then the reflection coefficient, and thus the stray radiation in the gyrotron, will also increase. In conclusion, for each mode pair and assuming the initial-design condition $R^{(2)} = 0$, the expression (6) allows for the reflection coefficient $R^{(1)}$ to be evaluated directly as a function of the eigenvalues of the two modes.

Besides the minimization of reflection of both operating modes from the diamond window, a second requirement is set by the electron gun and the quasi-optical system of the gyrotron. The operating $TE^{(1)}$ and $TE^{(2)}$ modes must have similar caustic radii, i.e.,

$$R_c^{(1)} = m_1 R_o/\chi^{(1)} \cong R_c^{(2)} = m_2 R_o/\chi^{(2)}, \quad (7)$$

to ensure efficient interaction with the electron beam produced by the gun and efficient conversion to a Gaussian RF beam by the quasi-optical system.

The requirement (7) and the minimization of the reflection coefficient $R^{(1)}$ in (6) form the basis for the search for appropriate mode pairs for dual-harmonic operation. Focusing on the operating frequencies of ~170 GHz for typical HCD operation and ~85 GHz for RI suppression, MW-class operation at the second cyclotron harmonic at ~170 GHz should be considered. As it will become clear in the next section and as has also been discussed in [9], targeting a power level above 1 MW would require an operating mode $TE^{(2)}$ with an eigenvalue above ~80, to be compatible with the Ohmic loading constraint for the outer cavity wall. Therefore, we considered the range $80 < \chi^{(2)} < 110$, to also avoid modes of very high order which are more prone to mode competition. Consequently, the eigenvalue of the $TE^{(1)}$ mode should be in the range $40 < \chi^{(1)} < 55$. Given that, a developed Python routine searched for operating mode pairs ($TE^{(2)}$, $TE^{(1)}$) with the appropriate eigenvalues and caustic radii. Under the two reasonable constraints of a maximum 1% difference in caustic radii in (7) ($|\delta R_c| < 1\%$) and a maximum 1% reflection for $TE^{(1)}$ ($R^{(1)} < 1\%$ in (6)), 51 mode pairs were identified.

A reduced list of 6 of the 51 identified mode pairs is shown in Table 1, corresponding to 6 representative cases. In particular, the pairs of Table 1 were chosen to represent the cases of lower and higher eigenvalues as well as the cases with a relative caustic radius R_c/R_o of ~0.3, ~0.4 and ~0.5. A relative caustic radius of around 0.3 is characteristic of "volume" modes and corresponds to typical coaxial-cavity gyrotrons [13–16]. In contrast, higher values than 0.5 correspond to more "whispering gallery" modes that are not a suitable choice for high power operation due to Ohmic loading considerations of the outer cavity wall [17]. Therefore, the mode pairs in Table 1 are considered sufficient to cover all relevant cases for this study.

Table 1
Reduced list of candidate mode pairs for dual - harmonic operation (Window thickness selected to achieve $R^{(2)} = 0$.).

$TE^{(2)}$/ $TE^{(1)}$	R_c/R_o	$\lvert\delta R_c\rvert$ (%)	$R^{(1)}$ (%)	$\chi^{(1)}$	$\chi^{(2)}$
$TE_{34,19}/TE_{17,10}$	0.32	0.77	0.23	53.0	105.1
$TE_{46,15}/TE_{23,8}$	0.43	0.79	0.24	53.9	106.9
$TE_{56,11}/TE_{28,6}$	0.53	0.85	0.29	52.9	104.8
$TE_{30,17}/TE_{15,9}$	0.32	0.87	0.30	47.1	93.3
$TE_{40,13}/TE_{20,7}$	0.43	0.91	0.32	46.7	92.5
$TE_{46,11}/TE_{23,6}$	0.49	0.94	0.34	46.8	92.8

2.2. Ohmic loading considerations

Besides the two requirements discussed in the previous Section, the thermal management of the Ohmic heating of the cavity walls imposes additional conditions on the selection of the operating modes. To ensure compatibility with CW operation, the Ohmic loading of both the outer cavity wall and the inner conductor must be below specific limits determined by the cooling technology. The expressions for the peak loading of the outer wall and of the inner rod (ρ_{out} and ρ_{in}, respectively), are given in [14]. The Ohmic loading increases significantly as the frequency f increases, so, in our case, ρ_{out} becomes critical first for the second-harmonic mode with $f^{(2)} \cong 2f^{(1)}$, assuming that the targeted RF power P_{out} generated in the cavity is the same for both harmonics. Additionally, the operating second-harmonic mode should be affected from the coaxial insert only slightly, to avoid excessive loading of the insert [9,14]. Because of this, for the second-harmonic mode the peak outer wall loading ρ_{out} can be approximated by its expression for a hollow cavity ρ_{hollow}:

$$\rho_{out} \cong \rho_{hollow} = Y(m,p,f)L_G P_{out} \quad (8)$$

The above generalized, geometry-independent expression for the peak value of ρ_{hollow} has been obtained following [14]. The function $Y(m, p, f)$ is a mode and frequency dependent coefficient and is defined in Appendix A, Eq. (A.1). In (8), the typical minimum value of the diffractive quality factor of the cavity has been assumed [18]:

$$Q_{dif,min} \approx 4\pi(L_G/\lambda)^2, \quad (9)$$

where L_G is the characteristic length of the Gaussian field profile of the mode. Of course, the actual value of Q_{dif} exceeds the minimum value, $Q_{dif,min}$. Therefore, (8) provides a minimum value for the peak outer wall loading. Regarding the characteristic length L_G for MW-class gyrotrons, typical values can be found in the literature: for example, L_G is approximately 7λ for a 1-MW 140-GHz gyrotron [19], 11λ for a 1.5-MW 140-GHz gyrotron [20], and 13λ for a > 1-MW 170-GHz second cyclotron harmonic gyrotron design [9].

For a first/second harmonic mode pair the Ohmic loading $\rho_{hollow}^{(1)}$ can be related to the Ohmic loading $\rho_{hollow}^{(2)}$ as

$$\rho_{hollow}{}^{(1)} \cong \rho_{hollow}{}^{(2)}/(2\sqrt{2}) \quad (10)$$

This can be deduced from (8), assuming comparable output power levels for both harmonics and considering the relations $m^{(2)} \cong 2m^{(1)}$, $\chi^{(2)} \cong 2\chi^{(1)}$, and $f^{(2)} \cong 2f^{(1)}$.

The constraints in ρ_{out} for the second-harmonic mode translate to constraints in the eigenvalue $\chi^{(2)}$. Fig. 1 shows a contour plot of $TE^{(2)}$ modes, where the x-axis represents the azimuthal index m_2 and the y-axis the radial index p_2. The colored contours represent ρ_{hollow} in kW/cm^2, calculated by (8) for every mode. The effective conductivity of the outer wall is set to $\sigma_{out} = 1.73\times 10^7$ S/m, corresponding to a typical correction factor of ~1.8 for the Ohmic losses, with respect to those in the case of ideal smooth copper at room temperature. Targeting ~1 MW of RF power at the gyrotron window, the cavity power P_{out} is set to 1.3 MW, to secure a good power margin. For any other desired value of P_{out}, the corresponding values of ρ_{hollow} scale proportionally. A characteristic length $L_G = 16\lambda^{(2)}$ has been chosen as an appropriate choice that enables effective interaction at both the first and second harmonic.

Fig. 1 is complemented by the contour plots of Fig. 2. The straight lines correspond to the relative caustic radii contours, indicating modes

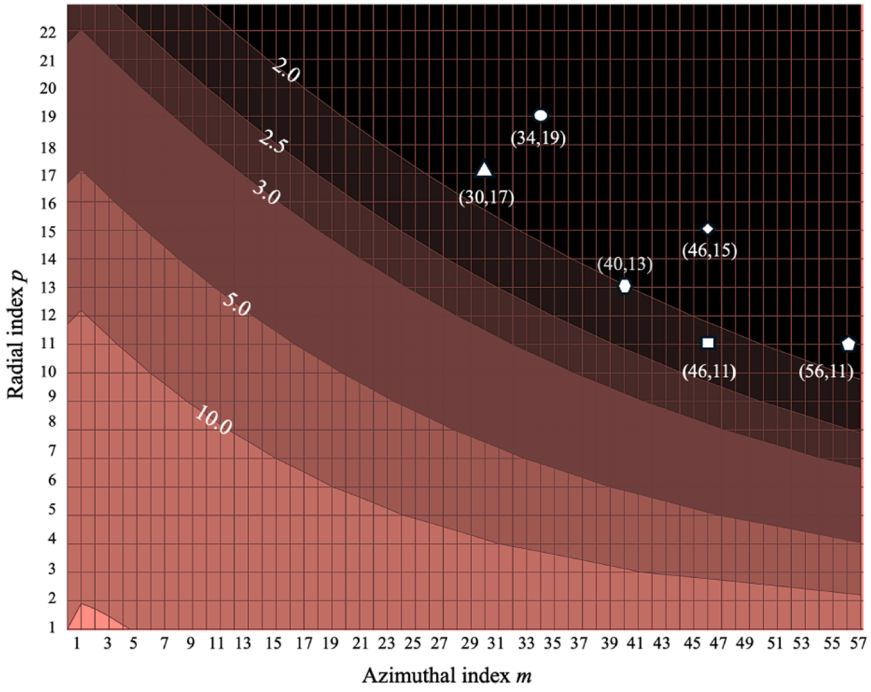


Fig. 1. Contour plot of the outer wall loading of $TE^{(2)}$ modes in the plane of the azimuthal index m_2 (x-axis) and the radial index p_2 (y-axis). The colored contours represent the Ohmic loading at the outer wall in kW/cm^2, assuming an effective electrical conductivity of $\sigma_{out} = 1.73\times 10^7$ S/m. The cavity is characterized by a length L_G=16$\lambda^{(2)}$. The cavity power is set to 1.3 MW at 170 GHz. The six $TE^{(2)}$ modes listed in Table 1 are included as labeled points.

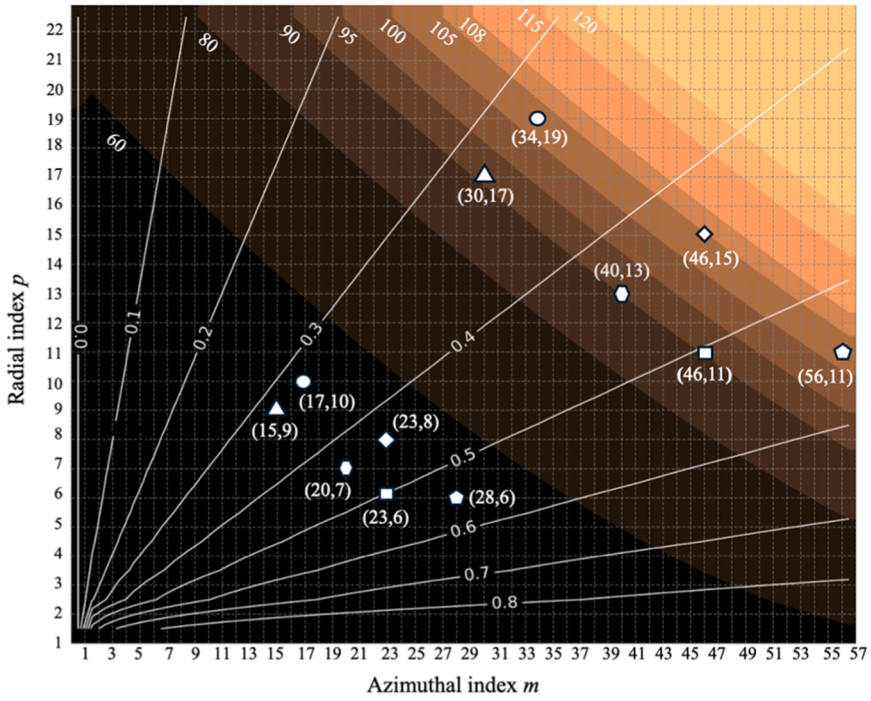


Fig. 2. Contour plot of the caustic radius and the eigenvalue of TE modes in the plane of the azimuthal index m (x-axis) and the radial index p (y-axis). The straight white lines denote the relative caustic radius R_c/R_o. The colored contours indicate the eigenvalues. The six mode pairs listed in Table 1 are also shown, using the same geometrical shape for each pair.

whose caustic radius is at the same distance from the outer wall. The colored contours represent the eigenvalues. From Figs. 1 and 2, it is apparent that the desired 1 MW, 170 GHz operation would require $TE^{(2)}$ modes with eigenvalue above ~80 to be in-line with the current technological limit of 2 - 2.5 kW/cm^2 for the outer wall loading [21], given that, as already mentioned, the expression (8) provides a minimum value for the outer wall loading. This validates our initial choice of $80 < \chi^{(2)} < 110$, used to obtain the mode pairs of Table 1.

The Ohmic loading ρ_{in} on the inner conductor should also be examined. In [14], an extensive study was conducted on the dependence

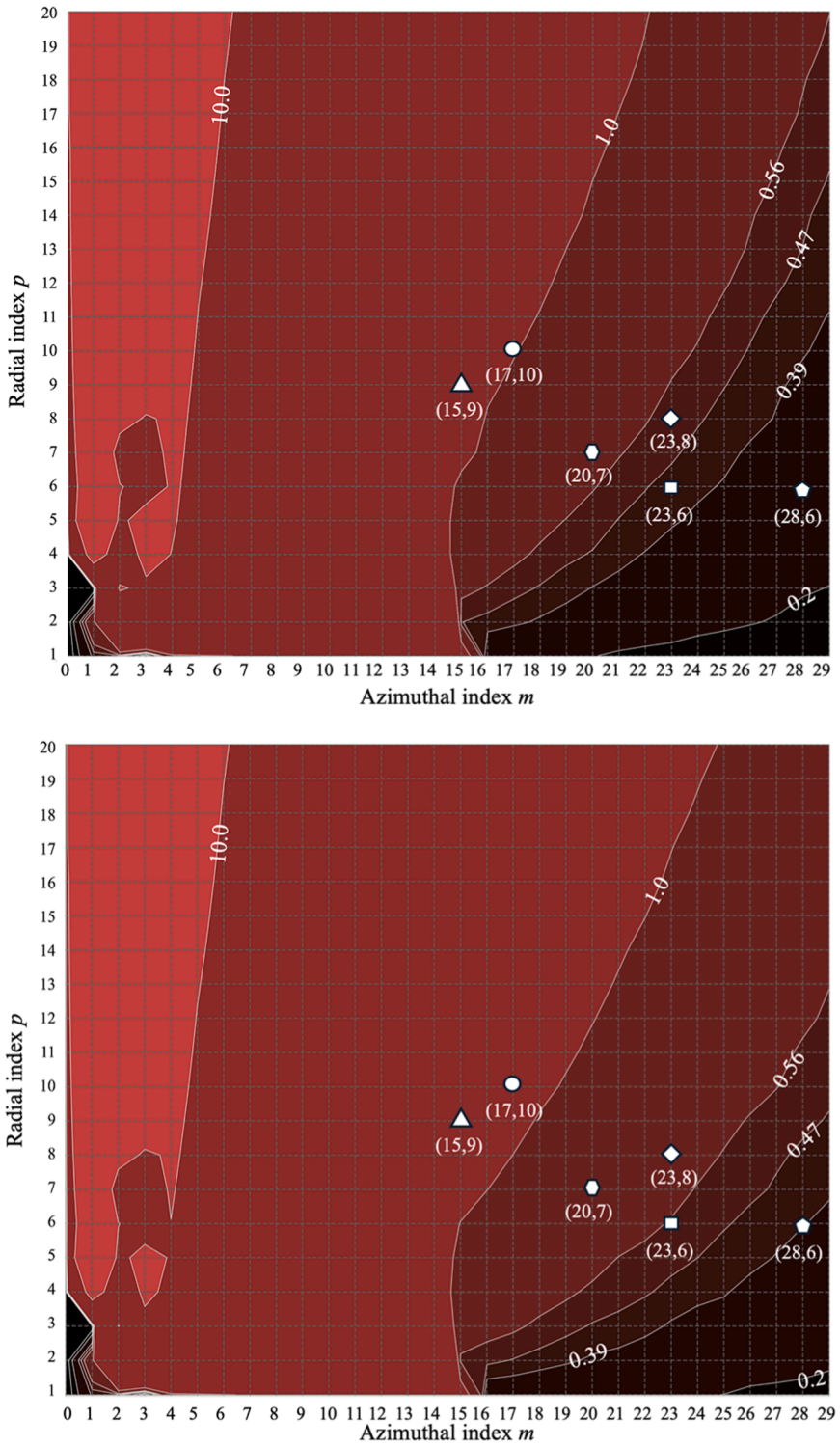


Fig. 3. Contour plot of $TE^{(1)}$ modes in the plane of the azimuthal index m_1 (x-axis) and the radial index p_1 (y-axis). The colored contours represent the Ohmic loading at the inner conductor of a coaxial insert characterized by a ratio $R_{ref} = 0.90$ (top) and $R_{ref} = 0.92$ (bottom), assuming a cavity power $P_{out} = 1.3$ MW. The six $TE^{(1)}$ modes listed in Table 1 are included as labeled points.

of the eigenvalue χ_{mp} and hence of ρ_{in} on the ratio $C = R_o/R_i$, where R_i is the inner-conductor radius. In the present study, the ratio C is expressed as $C = (\chi_{mp}/m)/R_{ref}$, where $R_{ref} = R_i/R_c$ and $R_c = R_o(m/\chi_{m,p})$. This approach enables ρ_{in} to be calculated independently from the cavity geometry, as every TE_{mp} mode perceives the coaxial insert - a highly conductive insert with longitudinal surface impedance corrugations - at the effective distance R_{ref}. Following [14] we can obtain:

$$\rho_{in} = \sqrt{\sigma_r}\,\frac{Q_{dif}}{Q_{dif,o}}\,\mathscr{F}\left(m,p,R_{ref}\right)\cdot\rho_{hollow} \tag{11}$$

where Q_{dif} and $Q_{dif,o}$ are the diffractive quality factors of the TE_{mp} mode in the coaxial and the corresponding hollow cavity, respectively. In the function $\mathscr{F}$ (defined in Appendix A, Eq. (A.3)) the corrugation depth d is chosen as $d/\lambda^{(2)} = 0.4$ and the width of slots to the period length L/S is assumed 0.5, as proposed in [14] to favor second-harmonic operation. Under these assumptions, $\mathscr{F}$ is dependent only on the TE_{mp} mode and the ratio R_{ref}.

The ratio R_{ref} should be chosen large enough, in order for the insert to suppress the dangerous first harmonic competing modes by decreasing their diffractive quality factors and enable operation at the second harmonic operating mode $TE^{(2)}$ [9,14,22]. However, there is an upper limit for R_{ref}, enforced by the requirement that the mode $TE^{(2)}$ should remain unaffected by the insert and induce an acceptable Ohmic load to the insert. Consequently, the ratio $Q_{dif}/Q_{dif,o}$ will be approximately unity for the $TE^{(2)}$ operating mode. On the other hand, although the $TE^{(1)}$ mode has a similar caustic radius as the mode $TE^{(2)}$, it is expected to be more influenced by the coaxial insert because the radial wavelength of $TE^{(1)}$ is about two times that of $TE^{(2)}$. This was shown in [9], where values of R_{ref} around 0.90 turned out to be the most appropriate for MW-class operation at the second harmonic. There, a ratio $Q_{dif}/Q_{dif,o} \sim 0.4$ was calculated for the first-harmonic competing modes that have a similar caustic radius (i.e. similar R_{ref}) with the operating second-harmonic mode. This indicates that the first-harmonic modes are strongly influenced by the insert, despite that the second-harmonic operating mode is unaffected by the insert.

The fact that the insert will influence the first harmonic modes can become critical for dual-harmonic gyrotrons because it means that the operating $TE^{(1)}$ mode can induce increased loading on the insert, preventing CW operation. This has been acknowledged in [23] and imposes an additional constraint on the selection of a mode-pair suitable for dual-harmonic operation. To quantify this constraint, contour plots of the insert loading ρ_{in} from the first harmonic operating mode $TE^{(1)}$ have been obtained using (11) and are shown in Fig. 3 for $R_{ref} = 0.90$ and $R_{ref} = 0.92$.

In Fig. 3 the colored contours represent ρ_{in} in kW/cm^2 for every mode, assuming $P_{out} = 1.3$ MW and $Q_{dif}/Q_{dif,o} \sim 0.4$ due to the insert. For $\rho^{(1)}_{hollow}$ we have used (10), setting $\rho^{(2)}_{hollow} = 2.5$ kW/cm^2 [21]. This choice was made to maximize the normalized field amplitude F and hence the interaction efficiency for the mode $TE^{(2)}$ [14]. Regarding the effective conductivity of the insert, we used $\sigma_{in} = 2.58 \times 10^7$ S/m, which correspond to a correction factor of 1.5. This is a finding obtained in [24] by multi-physics simulations of the loading of a coaxial insert made of Glidcop, with dimensions identical to the existing coaxial insert of the 170-GHz 2-MW short-pulse coaxial gyrotron at KIT [17]

In [24], it was also shown that such an insert is capable of withstanding a heat flux of up to 0.56 kW/cm^2. Assuming a mass flow rate of 2.5 l/min for the water, compatible with an acceptable pressure drop of 4.7 bar, the limiting factor is the temperature of the water, which should secure absence of boiling. Thus, the TE modes satisfying this constraint serve as candidate operating modes for CW MW-class dual-harmonic operation. A key observation from Fig. 3 is that the more "whispering gallery" modes (i.e. the modes with a larger caustic radius) are more suitable candidates for CW dual-harmonic operation. Specifically, the $TE^{(1)}$ modes with relative caustic radii of 0.5 (from Table 1) maintain an acceptable inner Ohmic loading, whereas the modes with relative caustic radii of 0.3 appear to exceed the limiting value of 0.56 kW/cm^2.

The same pattern of behavior for modes with a relative caustic radius of 0.3 and modes with a relative caustic radius of 0.5 is observed also for the $TE^{(2)}$ modes (Fig. 4). However, a $TE^{(2)}$ mode has a lower value of ρ_{in} than its $TE^{(1)}$ pair, despite the similarity of their caustic radii. Therefore, in a dual-harmonic coaxial gyrotron the loading of the insert due to the $TE^{(2)}$ mode will not be critical. As already discussed, this is a consequence of the $TE^{(1)}$ mode having twice the wavelength compared to its $TE^{(2)}$ mode pair, so the $TE^{(1)}$ mode is more affected by the coaxial insert.

2.3. Beam-wave interaction simulations

To complete the investigations on suitable mode pairs for CW MW-class dual-harmonic operation we reproduce the conclusions from the geometry-independent theoretical contour plots by performing beam-wave interaction simulations for 6 different specific cavities (a cavity for each mode pair from Table 1) designed to operate at 170/85 GHz. The simulations are performed using the European in-house code EURIDICE [25] and serve as an additional validation of the use of the generalized contour plots for the correct selection of operating mode pairs. In this part, a common reference framework has been established to ensure a consistent comparison of the results. The radius of the coaxial insert is selected to ensure that the ratio R_{ref} for the $TE^{(2)}/TE^{(1)}$ modes remains the same for all cases ($R_{ref} \sim 0.92$), providing an effective means to compare the maximum values of the Ohmic loading on the coaxial insert.

In Table 2, the coaxial insert radius and the parameters for all $TE^{(1)}$ candidate modes are summarized. With the value $R_{ref} = \sim 0.92$, a 60% reduction in the diffractive quality factor Q_{dif} of the $TE^{(1)}$ mode, compared to its value in the corresponding hollow cavity $Q_{dif,o}$, is achieved ($Q_{dif} \cong 0.4Q_{dif,o}$). For the operation at 170/85 GHz, a target of $P_{out} = 1.3$ MW has been set. An electron beam with a kinetic energy of 90 keV, 80 A beam current, and a velocity ratio (pitch factor) $\alpha = 1.3$ has been used, as the common operating point for all mode pairs, for comparison purposes. The outer wall loading ρ_{out} and the inner wall-loading ρ_{in} were also calculated by single-mode simulations with the $TE^{(2)}$ operating modes and are reported in Table 3.

The single-mode simulations confirm the conclusion from Fig. 3 (in which a ratio $R_{ref} = 0.92$ and a 60% reduction of Q_{dif} are also considered), since the $TE_{15,9}$ and $TE_{17,10}$ modes, with a relative caustic radius at 0.3, exceed significantly the acceptable value for ρ_{in}. Additionally, no $TE^{(2)}$ operating mode results in an unacceptable outer-wall loading at this output power, in agreement with the theoretical generalized plot of Fig. 1.

As shown from Tables 2 and 3, although a mode pair with a relative caustic radius at 0.3 reduces the heat flux on the outer wall, it causes severe heating of the coaxial insert during first-harmonic operation. This has already been acknowledged in [23], where the existing coaxial cavity of a short-pulse coaxial gyrotron at KIT, designed to operate at the second cyclotron harmonic, was investigated also for dual-harmonic operation with the $TE_{34,19}/TE_{17,10}$ mode pair. Therefore, modes with a relative caustic radius of 0.3 are probably not good candidates for CW dual-harmonic operation, unless a more effective insert cooling system is implemented.

According to Fig. 3 and Table 2, maintaining acceptable ρ_{in} at first harmonic operation with a mode pair characterized by a relative caustic radius of 0.4 is also questionable. Therefore, mode pairs with a relative caustic radius of 0.5 are more likely to support CW dual-harmonic operation. In the next section, a detailed cavity design is presented, capable of supporting CW operation and rapid switching between the two cyclotron harmonics.

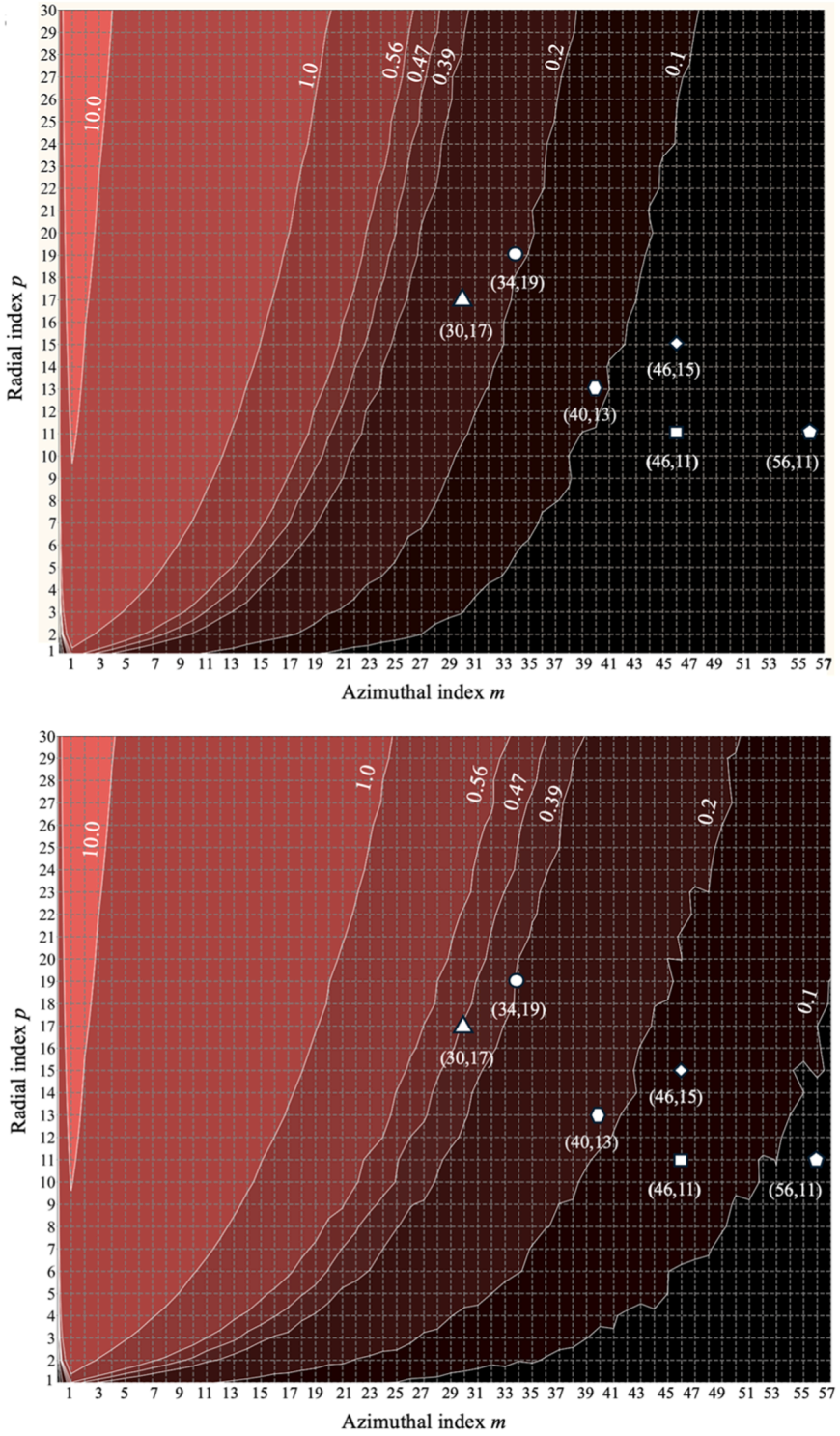


Fig. 4. Contour plot of $TE^{(2)}$ modes in the plane of the azimuthal index m_2 (x-axis) and the radial index p_2 (y-axis). The colored contours represent the Ohmic loading at the inner conductor of a coaxial insert characterized by a ratio $R_{ref} = 0.90$ (top) and $R_{ref} = 0.92$ (bottom), assuming a cavity power $P_{out} = 1.3$ MW. The six $TE^{(2)}$ modes listed in Table 1 are included as labeled points.

Table 2
Peak inner Ohmic loading from single-mode simulation of each candidate $TE^{(1)}$ mode for operation at $P_{out} = 1.3$ MW and 85 GHz with the corresponding coaxial insert radius and operating-mode parameters.

$TE^{(1)}$	$Q_{dif,o}$	Q_{dif}	R_c	R_i	ρ_{in} (kW/cm^2)
$TE_{17,10}$	797	319	9.47	8.7	1.2
$TE_{23,8}$	831	339	12.80	11.8	0.6
$TE_{28,6}$	896	358	15.58	14.4	0.4
$TE_{15,9}$	747	295	8.34	7.7	1.8
$TE_{20,7}$	795	338	11.12	10.1	0.9
$TE_{23,6}$	802	320	12.78	11.6	0.5

Table 3
Peak outer and inner Ohmic loading from single-mode simulation of each candidate $TE^{(2)}$ mode for operation at $P_{out} = 1.3$ MW and 170 GHz.

$TE^{(2)}$	$Q_{dif,o}$	Q_{dif}	ρ_{out} (kW/cm^2)	ρ_{in} (kW/cm^2)
$TE_{34,19}$	2912	3106	2.0	0.39
$TE_{46,15}$	2734	2863	1.8	0.14
$TE_{56,11}$	2756	2814	2.1	0.06
$TE_{30,17}$	2763	2955	2.1	0.33
$TE_{40,13}$	2765	2864	2.2	0.10
$TE_{46,11}$	2873	3058	2.2	0.12

3. Coaxial cavity design for CW dual-harmonic operation at 170/85 GHz

A coaxial cavity to provide high power CW dual-harmonic operation has been designed. The pair $TE_{46,11}/TE_{23,06}$, which has a relative caustic radius of 0.5, is chosen from the candidate mode pair list (Table 1) to be the operating mode pair, as explained in the previous section. It should be noted that the $TE_{56,11}/TE_{28,6}$ pair, also characterized by a relative caustic radius of 0.5, is less preferable because a denser spectrum of competing modes, due to higher eigenvalues, is expected in this case.

In Fig. 5, the coaxial cavity geometry and the assumed realistic magnetostatic field profile are presented. The design of the insert requires careful selection of the insert radius R_i and its taper angle φ_{coax}, for which multi-mode simulations are necessary. Stable operation with the $TE^{(2)}$ mode establishes the minimum R_i as well as the angle φ_{coax}, in order for the insert to adequately suppress the strong competition from first-harmonic modes and allow for second-harmonic operation. Stable operation with the mode $TE^{(1)}$ defines the maximum value of R_i, in order to avoid complete suppression of the $TE^{(1)}$ mode by the insert as well as excessive insert loading. Furthermore, the chosen beam radius R_b should correspond to a good coupling factor (Eq. 1 in [9]) for both modes $TE^{(1)}$ and $TE^{(2)}$.

The radius of the coaxial insert and the angle φ_{coax} (Fig. 5) are chosen to reduce by ~60% the diffractive quality factor of the $TE_{23,6}$ mode, compared to its value in the corresponding hollow cavity. The insert bears 92 longitudinal corrugations with a depth $d = 0.71$ mm ($d/\lambda^{(2)} = 0.4$) and $L/S = 0.5$. The corrugations occupy all the part of the inner conductor in Fig.5. The optimum radius of the coaxial insert was found at $R_{ref} = 0.92$, since larger insert radii suppress the $TE^{(1)}$ operating mode. The beam radius is set to $R_b = 13.2$ mm, which is considered a good compromise, resulting in 8.2% lower coupling factor for the mode $TE^{(1)}$ and in 1.5% lower coupling factor of the $TE^{(2)}$ mode, as compared to the optimal values. The chosen R_b is a sub-optimal beam radius for each mode because the optimal coupling of a first-harmonic mode occurs at a larger beam radius than the one of the corresponding second-harmonic mode. The adjustment of the beam radius to the optimal value for each mode would require a small adjustment of the magnetic field during operation, which is possible only in a time frame of the order of 1 s. Since this study focuses on rapid switch (in the ms range) between the two harmonics, the above compromise with respect to the beam-wave coupling factor is necessary.

The excitation of the second-harmonic mode and the rapid switch to the first harmonic mode can be realized by changing the electrode voltages in a triode-type electron gun. In such a gun, the electron energy and the pitch factor α can, in principle, be controlled independently by changing the voltage of the anode and the modulation anode. For the usual high-power supplies for gyrotrons, the changes in the voltage can be achieved in the ms time scale.

A conceptual triode-type start-up and an appropriate fast-switching scenario, verified by realistic simulations with EURIDICE, is presented in Fig. 6. Multi-mode simulations (75 modes, including possible parasitic backward-wave modes [26]) of the beam-wave interaction were performed for the mode pair $TE_{46,11}/TE_{23,6}$. The right axis in Fig. 6 shows the pitch factor α (multiplied by 100) and the beam kinetic energy in keV. The bottom graph uses a logarithmic scale to show power levels in the range 0–100 kW and illustrates that the operation is free of parasitic modes.

The strategy followed is to start by setting the cathode voltage and the anode voltage such that an electron beam with kinetic energy $E_b = 75$ keV enters the cavity region ($t = 0$). The modulation-anode voltage is set to a value that leads to an initial pitch factor $\alpha \sim 0.6$. With these parameters there is no excitation of any mode. Then α is increased until it reaches its nominal value of $\alpha = 1.29$ ($t = 500$), achieving the excitation of the mode $TE_{23,6}$ at ~86 GHz. Then, the beam energy is also increased but keeping the pitch factor constant at its

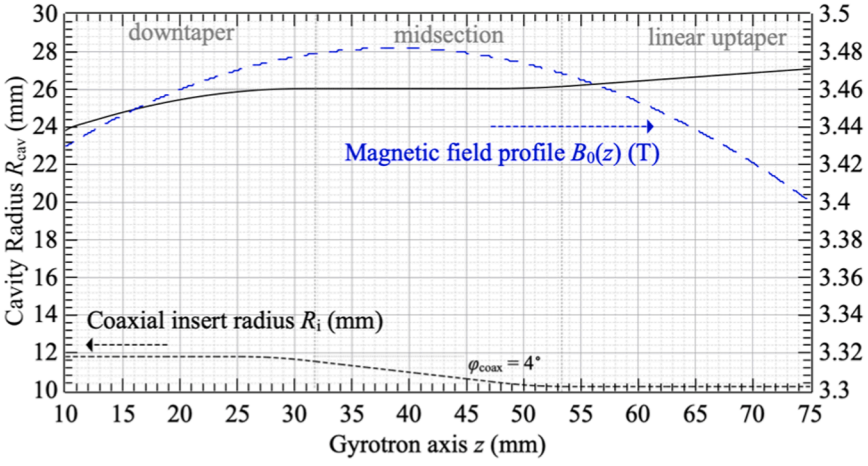


Fig. 5. The simulated coaxial cavity, designed to operate at 170/85 GHz. The magnetic field profile is shown on the right axis. The x-axis represents the axis z of the gyrotron in mm.

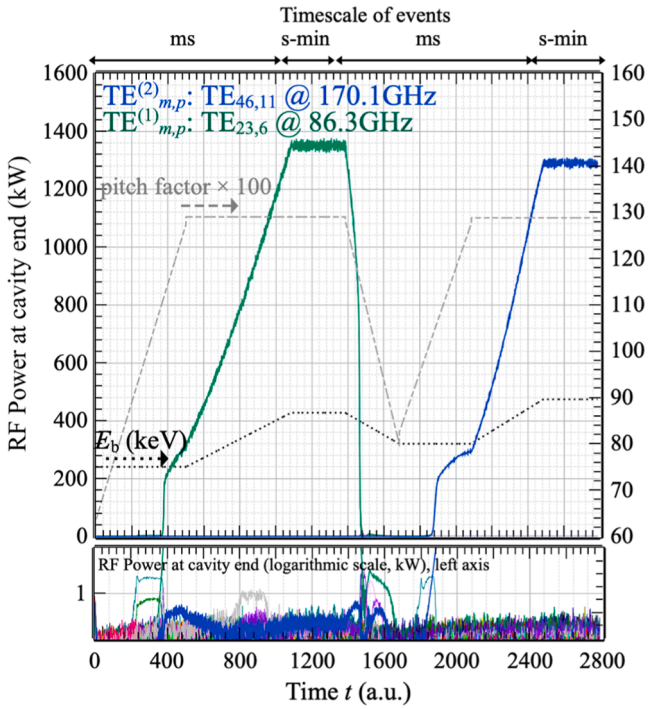


Fig. 6. Multi-mode simulation (75 modes) of the beam-wave interaction showing the excitation scenario, stable operation, and fast switching scenario for the mode pair $TE_{46,11}/TE_{23,6}$. The right axis shows the pitch factor (multiplied by 100) and the beam kinetic energy in keV. The bottom graph uses a logarithmic scale to show power levels in the range 0–100 kW and illustrates that the operation is free of parasitic modes. The duration of each event is shown at the top of the graph.

nominal value. When the nominal $E_b = 86.7$ keV is reached, stable operation with the $TE_{23,6}$ mode at $P_{out} = 1.35$ MW is demonstrated by keeping all the beam parameters constant.

To switch to second-harmonic operation with the $TE_{46,11}$ mode at 170 GHz, the fast-switching scenario is the following: The beam energy is decreased by 6 keV, while the pitch factor is decreased to $\alpha = 0.6$. This process can, in principle, occur rapidly, since the accelerating voltage and the modulation-anode voltage can be adjusted within some μs per kV. The above change in beam energy and pitch factor leads to the detuning of the $TE_{23,6}$ mode ($t = 1500$). To excite the $TE_{46,11}$ mode, the pitch factor needs to be increased to its nominal value $\alpha = 1.3$ ($t = 2100$) and remain stable afterwards. The $TE_{46,11}$ mode attains an output power of 1.3 MW when E_b is increased from 80 keV to approximately 90 keV. Stable operation for this mode is also demonstrated ($t = 25{,}00$-2800).

Table 4
Operating point and calculated performance for the $TE_{46,11}/TE_{23,6}$ mode pair.

	$TE_{46,11}$	$TE_{23,6}$
Electron beam energy (keV)	89.6	86.7
Electron beam current (A)	74	72
Magnetic field (T)	3.482	
Pitch factor α	1.28	1.29
Electron beam radius (mm)	13.2	
α – spread (rms)	15%	
Kinetic energy spread (rms)	0.1%	
Guiding center spread	2 Larmor radii	
Cavity power P_{out} (MW)	1.3	1.35
Frequency (GHz)	170.0	86.1
Maximum outer Ohmic loading* (kW/cm^2)	2.4	0.7
Maximum inner Ohmic loading** (kW/cm^2)	0.12	0.54
Electronic efficiency	20%	22%

*Assuming a correction factor of 1.8 w.r.t. ideal copper at room temperature [9].
**Assuming a correction factor of 1.5 w.r.t. ideal copper at room temperature [24].

The performance and the nominal beam parameters for each mode are summarized in Table 4. Note that a realistic spread of 15% in the pitch factor α and typical values of spreads for the energy and the guiding center have been considered.

As can be seen in Fig. 6, the operation is free of parasitic modes. Higher values for the pitch factor resulted in parasitic mode excitation. Therefore, parasitic backward wave oscillations set the threshold for the pitch factor below 1.3, resulting in an electronic efficiency of 20–22% for both harmonics. Such values for the electronic efficiency, defined as the average electron energy loss by the beam-wave interaction, are typically expected for MW-class second-harmonic operation [9]. The interaction at the second cyclotron harmonic is characterized by reduced electronic efficiency since, for a given RF field amplitude, the interaction at higher harmonics is inherently weaker than the interaction at the fundamental. For the MW-class operation at the fundamental cyclotron frequency, however, the electronic efficiency reported in Table 4 is significantly reduced compared to the typical values of ~35% [21]. This is an unavoidable compromise in the dual-harmonic concept, because the fundamental mode should not dominate or suppress the second-harmonic mode and hence, the quality factor of the $TE^{(1)}$ mode is significantly reduced by the presence of the coaxial insert. Modifications on the outer cavity wall can increase the diffractive quality factor of all modes. However, the increase in Q_{dif} is associated with higher ohmic losses on the outer wall, exceeding - in the case of $TE_{46,11}$ - the current technological limit of 2.5 kW/cm^2.

Apparently, the dual-harmonic concept has an impact on the interaction efficiency for both operating modes. To bring the overall gyrotron efficiency to levels compatible with the needs of a fusion reactor, a multi-stage depressed collector should be considered for dual-harmonic gyrotrons [27]. The increased efficiency results from the use of multiple deceleration potentials, which separate the spent-beam electrons based on their kinetic energy. Therefore, in the collector design, the spent-beam energy spectrum for both harmonics should be taken into account for the dual-harmonic gyrotron. As pointed out in [28], the overall efficiency of a high-power 2nd harmonic gyrotron design with interaction efficiency of the order of 20% could reach 50% with a proper multi-stage depressed collector design.

4. Summary and conclusions

In this paper, the feasibility of coaxial gyrotron cavities with longitudinally corrugated inner conductor to support MW-class CW dual-harmonic operation and to seamlessly switch fast between operation at the fundamental cyclotron frequency and at the second cyclotron harmonic was theoretically investigated.

The two operating modes are required to have similar caustic radii, with a frequency ratio as close as possible to two. Specific criteria and routines for the identification of suitable operating mode pairs were developed. Additionally, a generalized model capable of foreseeing the behavior of the Ohmic loading prior to designing and simulating the coaxial cavity was proposed and showed that a relative caustic radius of ~0.5 for the operating mode pair is highly beneficial for MW-class dual-harmonic operation.

On this basis, a coaxial cavity was designed, capable of delivering 1.35 MW at 85 GHz, operating with the fundamental mode $TE_{23,6}$, with 22% electronic efficiency and with an Ohmic loading of 0.7 kW/cm^2 for the outer cavity wall and 0.54 kW/cm^2 for the coaxial insert. Operating with the second-harmonic mode $TE_{46,11}$, a power of 1.3 MW is reached at 170 GHz with 20% electronic efficiency and with an Ohmic loading of 2.4 kW/cm^2 for the outer wall and 0.12 kW/cm^2 for the coaxial insert. A rapid (ms range) switching scenario using a triode-type electron gun was also demonstrated by realistic multi-mode simulations.

The realization of such dual-harmonic gyrotrons would provide a new degree of flexibility in EC HCD system design in fusion reactors, reducing the number of gyrotrons and transmission lines required and simplifying the overall architecture of the system.

CRediT authorship contribution statement

Elena Katsara: Writing – review & editing, Writing – original draft, Validation, Methodology, Investigation, Formal analysis, Conceptualization. **Konstantinos A. Avramidis:** Writing – review & editing, Supervision, Methodology, Conceptualization. **Ioannis Chelis:** Writing – review & editing. **Chuanren Wu:** Writing – review & editing, Conceptualization. **Jianbo Jin:** Validation, Investigation. **Lukas Feuerstein:** Writing – review & editing, Investigation. **Charilaos Argyropoulos:** Writing – review & editing, Validation, Investigation. **Manfred Thumm:** Writing – review & editing. **Stefan Illy:** Writing – review & editing, Project administration.

Declaration of competing interest

The authors declare that they have no known competing financial interests or personal relationships that could have appeared to influence the work reported in this paper.

Acknowledgments

This work has been carried out within the framework of the EUROfusion Consortium, funded by the European Union via the Euratom Research and Training Programme (Grant Agreement No 101052200 – EUROfusion). Views and opinions expressed are however those of the author(s) only and do not necessarily reflect those of the European Union or the European Commission. Neither the European Union nor the European Commission can be held responsible for them. Part of the simulations have been performed at the EUROfusion High Performance Computing facilities at Cineca (Marconi, Leonardo, and Pitagora).

Appendix A

Following [14], and assuming $Q_{\mathrm{dif,min}} \approx 4\pi(L_G/\lambda)^2$, we obtain $\rho_{\mathrm{hollow}} = Y(m, p, f)L_G P_{\mathrm{out}}$, where

$$Y(m,p,f) = 8\pi^3 \cdot \frac{\delta_{out}}{Z_0 (c/f)^4} \frac{0,1914}{\chi_{mp,o}^2 - m^2} \tag{A.1}$$

In the function Y, $\delta_{\mathrm{out}} = [2/(\mu_0 \sigma_{\mathrm{out}} \omega)]^{1/2}$ is the skin depth for the outer wall, which has an effective conductivity σ_{out}, and $Z_0 \equiv \mu_0 c$ is the free-space wave impedance. $\chi_{mp,o}$ is the eigenvalue of the TE_{mp} mode in the corresponding hollow cavity.

The maximum Ohmic loading on the coaxial insert ρ_{in} is given from (6) in [14]. From that, and for a mode close to cutoff, we can obtain:

$$\rho_{\mathrm{in}} = \sqrt{\sigma_{\mathrm{r}}} \frac{Q_{\mathrm{dif}}}{Q_{\mathrm{dif,o}}} \mathscr{F}(m,p,R_{\mathrm{ref}}) \cdot \rho_{\mathrm{hollow}} \tag{A.2}$$

where $\sigma_r = \sigma_{\mathrm{out}}/\sigma_{\mathrm{in}}$ (σ_{in} is the effective conductivity of the insert) and the function $\mathscr{F}$ is defined as:

$$\mathscr{F}(m,p,R_{\mathrm{ref}}) = \frac{\pi C_{mp}^2 Z_{mp}^2 (mR_{\mathrm{ref}})}{\cos^2\left(2\pi\left(\frac{d}{\lambda}\right)\left(\frac{\chi_{mp}}{\chi_{mp,0}}\right)\right)} \cdot \left(\chi_{mp}^2 - m^2\right) \tag{A.3}$$

The normalization coefficient C_{mp} is given by

$$\frac{1}{\pi C_{mp}^2} = Z_{mp}^2(\chi_{mp})\left[\chi_{mp}^2 - m^2\right] + Z_{mp}^2\left(\frac{\chi_{mp}}{C}\right) \cdot \left\{ m^2 - \left(\frac{\chi_{mp}}{C}\right)^2 (1 + w^2) + \frac{\chi_{\mathrm{mp}}}{\mathrm{C}} \left[\mathrm{w} + 2\pi\left(\frac{\mathrm{d}}{\lambda}\right)\left(\frac{\chi_{\mathrm{mp}}}{\chi_{\mathrm{mp,o}}}\right)\left(\frac{1}{\mathrm{s}} + \frac{\mathrm{s}}{\mathrm{l}}\,\mathrm{w}^2\right)\right]\right\}, \tag{A.4}$$

where $w = (L/S)\tan[2\pi\left(\frac{d}{\lambda}\right)\left(\frac{\chi_{mp}}{\chi_{mp,o}}\right)]$ is the corrugation parameter and $Z_{mp}(u) = J_m(u) - [J'_m(\chi_{mp})/Y'_m(\chi_{mp})]Y_m(u)$ is a linear combination of Bessel and Neumann functions.

Data availability

Data will be made available on request.

References

[1] M. Thumm, State-of-the-art of high-power gyro-devices: 2025 update of experimental results, J. Infrared Millim. Terahz. Waves 46 (2025), https://doi.org/10.1007/s10762-025-01042-y.

[2] T. Franke, G. Aiello, K. Avramidis, C. Bachmann, B. Baiocchi, C. Baylard, A. Bruschi, D. Chauvin, A. Cufar, R. Chavan, C. Gliss, F. Fanale, L. Figini, G. Gantenbein, S. Garavaglia, G. Granucci, J. Jelonnek, G. Suárez López, A. Moro, M. Moscheni, N. Rispoli, M. Siccinio, P. Spaeh, D. Strauss, F. Subba, I. Tigelis, M. Q. Tran, C. Tsironis, C. Wu, H. Zohm, Integration concept of an electron cyclotron system in DEMO, Fusion Eng. Des. 168 (2021) 112653, https://doi.org/10.1016/j.fusengdes.2021.112653.

[3] E.V. Suvorov, W. Kasparek, L.V. Lubyako, N.K. Skalyga, V. Erckmann, T. Laqua, Gyrotron as a source of probing radiation for collective Thomson scattering experiments, in: Third International Kharkov Symposium "Physics and Engineering of Millimeter and Submillimeter Waves", MSMW'98, Kharkov, Ukraine, 1998, pp. 188–190, https://doi.org/10.1109/MSMW.1998.758947.

[4] D. Moseev, H.P. Laqua, T. Stange, I. Abramovic, S.K. Nielsen, S. Äkäslompolo, K. Avramidis, H. Braune, G. Gantenbein, S. Illy, J. Jelonnek, J. Jin, W. Kasparek, L. Krier, S.B. Korsholm, C. Lechte, A. Marek, S. Marsen, M. Nishiura, I. Pagonakis, M. Salewski, J. Rasmussen, A. Tancetti, M. Thumm, R.C. Wolf, W7-X Team, Collective Thomson scattering diagnostic for Wendelstein 7-X at 175 GHz, J. Instrum. 15 (2020) C05035, https://doi.org/10.1088/1748-0221/15/05/C05035.

[5] M. Siccinio, W. Biel, E. Fable, T. Franke, F. Janky, P.T. Lang, M. Mattei, F. Maviglia, F. Palermo, O. Sauter, M.Q. Tran, S. Van Mulders, H. Zohm, Impact of the plasma operation on the technical requirements in EU-DEMO, Fusion Eng. Des. 179 (2022) 113123, https://doi.org/10.1016/j.fusengdes.2022.113123.

[6] P. Späh, HCD SRD for FP9, EUROfusion IDM document EFDA_D_2NV496 v3.2. https://idm.euro-fusion.org/?uid=2NV496, 2022.

[7] S. Illy, ENR-TEC.02.KIT-T001-D001 — Intermediate report, KIT; NCSRD, 2S4NTZ v1.0. https://idm.euro-fusion.org/?uid=2S4NTZ, 2024.
[8] S. Illy, K.A. Avramidis, I. Chelis, B. Ell, L. Feuerstein, G. Gantenbein, Z. Ioannidis, J. Jelonnek, J. Jin, G. Latsas, A. Marek, D. Peponis, T. Rzesnicki, M. Thumm, I. Tigelis, C. Wu, Progress in the design of megawatt-class fusion gyrotrons operating at the second harmonic of the cyclotron frequency, in: 2023 48th Int. Conf. Infrared, Millimeter, and Terahertz Waves (IRMMW-THz), 2023, https://doi.org/10.1109/IRMMW-THz57677.2023.10299170.
[9] I.G. Chelis, K.A. Avramidis, D.V. Peponis, I.G. Tigelis, High-frequency MW-class coaxial gyrotron cavities operating at the second cyclotron harmonic, IEEE Trans. Electron. Devices 71 (2024) 2140–2146, https://doi.org/10.1109/TED.2024.3356472.
[10] J. Franck, Systematic Study of Key Components for a Coaxial-Cavity Gyrotron for DEMO, KIT Scientific Publishing, Karlsruhe, 2017, https://doi.org/10.5445/KSP/1000068000.
[11] H.-U. Nickel, Hochfrequenztechnische Aspekte zur Entwicklung rückwirkungsarmer Ausgangsfenster Für Millimeterwellengyrotrons hoher Leistung, Universität Karlsruhe (TH, 1995, https://doi.org/10.5445/IR/46595. PhD thesis.
[12] M. Thumm, Development of output windows for high-power long-pulse gyrotrons and EC wave applications, Int. J. Infrared Millim. Waves 19 (1998) 3–14, https://doi.org/10.1023/A:1022514528711.
[13] T. Ruess, G. Gantenbein, Z. Ioannidis, T. Rzesnicki, D. Wagner, M. Thumm, J. Jelonnek, Frequency and mode measurement techniques for megawatt-class gyrotrons, Technisches. Messen. 89 (2022) 85–96, https://doi.org/10.1515/teme-2021-0039.
[14] K.A. Avramidis, C.T. Iatrou, J.L. Vomvoridis, Design considerations for powerful continuous-wave second-cyclotron-harmonic coaxial-cavity gyrotrons, IEEE Trans. Plasma Sci. 32 (2004) 917–928, https://doi.org/10.1109/TPS.2004.828781.
[15] B. Piosczyk, M. Thumm, M. Kuntze, G. Michel, J. Jelonnek, M. Schlechtweg, T. Idehara, Coaxial cavity gyrotron with dual RF beam output, IEEE Trans. Plasma Sci. 26 (1998) 393–401, https://doi.org/10.1109/27.700770.
[16] P.C. Kalaria, Feasibility and Operational Limits for a 236 GHz Hollow-Cavity Gyrotron for DEMO, KIT Scientific Publishing, Karlsruhe, 2017, https://doi.org/10.5445/KSP/1000073581.
[17] T. Rzesnicki, B. Piosczyk, S. Kern, S. Illy, J. Jin, A. Samartsev, A. Schlaich, M. Thumm, 2.2-MW record power of the 170-GHz European preprototype coaxial-cavity gyrotron for ITER, IEEE Trans. Plasma Sci. 38 (2010) 1141–1149, https://doi.org/10.1109/TPS.2010.2040842.
[18] G.S. Nusinovich, Introduction to the Physics of Gyrotrons, Johns Hopkins University Press, 2004, https://doi.org/10.1353/book.62236.
[19] V. Erckmann, P. Brand, H. Braune, G. Dammertz, G. Gantenbein, W. Kasparek, H. P. Laqua, H. Maassberg, N.B. Marushchenko, G. Michel, M. Thumm, Y. Turkin, M. Weissgerber, A. Weller, W7-X ECRH Team at IPP Greifswald, W7-X ECRH Team at FZK Karlsruhe, W7-X ECRH Team at IPF Stuttgart, electron cyclotron heating for W7-X: physics and technology, Fusion Sci. Technol 52 (2007) 291–312, https://doi.org/10.13182/FST07-A1508.
[20] S. Ponomarenko, H.P. Laqua, K.A. Avramidis, G. Gantenbein, J. Gontard, F. Hollmann, S. Illy, Z.C. Ioannidis, J. Jelonnek, J. Jin, S. Kohler, L. Krier, A. Leggieri, F. Legrand, G. Lietaer, C. Lievin, S. Marsen, D. Moseev, F. Noke, T. Rzesnicki, T. Stange, M. Thumm, R.C. Wolf, Experimental results of the novel 1.5-MW-class 140-GHz continuous-wave gyrotron for Wendelstein 7-X stellarator, IEEE Electron. Device Lett. 45 (2024) 2550–2553, https://doi.org/10.1109/LED.2024.3484218.
[21] M.K.A. Thumm, G. Denisov, K. Sakamoto, M.Q. Tran, High-power gyrotrons for electron cyclotron heating and current drive, Nucl. Fusion 59 (2019) 073001, https://doi.org/10.1088/1741-4326/ab2005.
[22] L. Feuerstein, K.A. Avramidis, I. Chelis, B. Ell, S. Illy, J. Jelonnek, E. Katsara, D. Peponis, A. Schmidt, M. Thumm, I. Tigelis, N. Wirth, C. Wu, Enhanced suppression of first harmonic competing modes in harmonic coaxial gyrotron cavities with tapered corrugation depth, J. Infrared Millim. Terahz. Waves 47 (2026) 21, https://doi.org/10.1007/s10762-026-01128-1.
[23] E. Katsara, K.A. Avramidis, I. Chelis, Z. Ioannidis, L. Feuerstein, C. Wu, C. Argyropoulos, S. Illy, Possibilities for dual-harmonic high-power operation of a coaxial gyrotron cavity, in: 2026 17th German Microwave Conference (GeMiC), Karlsruhe, Germany, 2026, pp. 85–88, https://doi.org/10.1109/GeMiC71240.2026.11516477.
[24] K.A. Avramidis, E. Katsara, Report on the investigations on the limits of the ohmic loading of the coaxial insert and on new cavity cooling concepts: electrodynamic part, HCD-T.02.01-T030-D005, EUROfusion IDM Document 2S88FF (2022). https://idm.euro-fusion.org/?uid=2S88FF.
[25] K.A. Avramidis, I.G. Pagonakis, C.T. Iatrou, J.L. Vomvoridis, EURIDICE: a code-package for gyrotron interaction simulations and cavity design, EPJ. Web. Conf. 32 (2012) 04016, https://doi.org/10.1051/epjconf/20123204016.
[26] K.A. Avramidis, A. Marek, I. Chelis, Z.C. Ioannidis, L. Feuerstein, J. Jelonnek, M. Thumm, I. Tigelis, Simulation of parasitic backward-wave excitation in high-power gyrotron cavities, IEEE Trans. Electron. Devices 70 (2023) 1898–1905, https://doi.org/10.1109/TED.2023.3242216.
[27] B. Ell, C. Wu, G. Gantenbein, S. Illy, M. Misko, I.G. Pagonakis, J. Weggen, M. Thumm, J. Jelonnek, Toward the first continuous wave compatible multistage depressed collector design for high power gyrotrons, IEEE Trans. Electron. Devices 70 (2023) 1299–1305, https://doi.org/10.1109/TED.2023.3234885.
[28] S. Illy, K.A. Avramidis, I. Chelis, B. Ell, L. Feuerstein, G. Gantenbein, Z. Ioannidis, J. Jelonnek, J. Jin, E. Katsara, G. Latsas, A. Marek, D. Peponis, T. Rzesnicki, M. Thumm, I. Tigelis, C. Wu, Technical concepts for megawatt-class fusion gyrotrons operating at the second harmonic of the cyclotron frequency, in: 2025 26th International Vacuum Electronics Conference (IVEC), 2025, pp. 1–2, https://doi.org/10.1109/IVEC63678.2025.11115490.